Magnetic Resonance Materials in Physics, Biology and Medicine
https://doi.org/10.1007/s10334-017-0668-2

RESEARCH ARTICLE

Cardiac magnetic resonance T1 and extracellular volume mapping with motion correction and co-registration based on fast elastic image registration

Shuo Zhang[1,2] · Thu Thao Le[1] · Sven Kabus[3] · Boyang Su[1] · Derek J. Hausenloy[1,4,5,6] · Stuart A. Cook[1,4] · Calvin W. L. Chin[1,4] · Ru San Tan[1]

Received: 6 June 2017 / Revised: 5 November 2017 / Accepted: 25 November 2017

Abstract

Objective Our aim was to investigate the technical feasibility of a novel motion compensation method for cardiac magntic resonance (MR) T1 and extracellular volume fraction (ECV) mapping.

Materials and methods Native and post-contrast T1 maps were obtained using modified look-locker inversion recovery (MOLLI) pulse sequences with acquisition scheme defined in seconds. A nonrigid, nonparametric, fast elastic registration method was applied to generate motion-corrected T1 maps and subsequently ECV maps. Qualitative rating was performed based on T1 fitting-error maps and overlay images. Local deformation vector fields were produced for quantitative assessment. Intra- and inter-observer reproducibility were compared with and without motion compensation.

Results Eighty-two T1 and 39 ECV maps were obtained in 21 patients with diverse myocardial diseases. Approximately 60% demonstrated clear quality improvement after motion correction for T1 mapping, particularly for the poor-rating cases (23% before vs 2% after). Approximately 67% showed further improvement with co-registration in ECV mapping. Although T1 and ECV values were not clinically significantly different before and after motion compensation, there was improved intra- and inter-observer reproducibility after motion compensation.

Conclusions Automated motion correction and co-registration improved the qualitative assessment and reproducibility of cardiac MR T1 and ECV measurements, allowing for more reliable ECV mapping.

Keywords T1 relaxation time · Extracellular volume · Motion correction · Co-registration · Diffuse fibrosis

Abbreviations

CMR	Cardiovascular magnetic resonance
bSSFP	Balanced steady-state free precession
ECG	Electrocardiogram
ECV	Extracellular volume fraction
LGE	Late gadolinium enhancement
LV	Left ventricular
MOLLI	Modified look-locker inversion recovery
T1	Longitudinal relaxation time constant

Shuo Zhang, Thu Thao Le, Calvin W. L. Chin and Ru San Tan contributed equally.

Electronic supplementary material The online version of this article (https://doi.org/10.1007/s10334-017-0668-2) contains supplementary material, which is available to authorized users.

✉ Shuo Zhang
zhangshuo517@gmail.com

[1] National Heart Centre Singapore, 5 Hospital Drive, Singapore 169609, Singapore

[2] Philips Healthcare Singapore, 622 Lorong 1, Singapore 319763, Singapore

[3] Philips Research, Röntgenstrasse 24-26, 22335 Hamburg, Germany

[4] Duke-NUS Medical School, 8 College Road, Singapore 169857, Singapore

[5] The Hatter Cardiovascular Institute, University College London, London, UK

[6] The National Institute of Health Research University College London Hospitals Biomedical Research Centre, London, UK

Published online: 21 December 2017

Introduction

Myocardial fibrosis is one of the histological hallmarks of left-ventricular decompensation [1]. Although myocardial biopsy is the gold standard for diagnosing fibrosis, the procedure is invasive and susceptible to sampling error. Instead, late gadolinium-enhanced imaging, a conventional cardiovascular magnetic resonance (CMR) technique, offers accurate detection of focal regions of myocardial fibrosis. However, this form of fibrosis commonly occurs late in the disease process and is not believed to be reversible [2, 3]. Recent advances in myocardial T1 mapping allow quantification of more diffuse types of fibrosis, which are potentially reversible with targeted therapies [4]. Conversely, unlike native (non-contrast) myocardial T1 that reflects disease involving both the cardiomyocyte and interstitium, extracellular volume fraction (ECV) directly estimates interstitial expansion [5]. In the absence of amyloid deposition and edema, ECV correlates with the amount of myocardial fibrosis on histology [6, 7]. Moreover, recent data have also demonstrated an important prognostic association between ECV and adverse outcomes, independent of traditional predictors such as ejection fraction, age, and coronary artery disease [4, 8].

State-of-the-art CMR for quantitative T1 mapping relies on electrocardiogram (ECG)-triggered acquisitions following initial magnetization preparation, e.g., inversion recovery (IR). One of the most widely used methods is the modified look-locker inversion recovery (MOLLI) technique [9]. However, all clinically available techniques, including MOLLI, result in a series of images across multiple heart beats within one breath hold, which is susceptible to motion artifacts caused by inconsistent breath-holding and varying cardiac cycles. Furthermore, current ECV estimation relies on cumbersome measurement of myocardial and blood-pool T1 before and after gadolinium contrast administration, rendering it prone to image misalignment due to two separate acquisitions. Therefore, an automated process of motion correction and co-registration of native and post-contrast images, as well as maps, is critical for developing T1 and ECV mapping for clinical applications. Despite previous works [10, 11], such an approach remains unavailable universally in clinical practice on all vendor platforms. The purpose of this work was to investigate the technical feasibility and clinical performance of a novel straightforward and robust approach for motion compensation at 3T.

Materials and methods

Patients

Twenty-one patients [18 men, 3 women, age range 17–71 (mean 47 ± 18) years] with diverse cardiac pathologies underwent CMR on a 3T system (Ingenia, Philips Healthcare, Best, The Netherlands) with a maximum 28-channel body (12-channel spine, 16-channel torso) coil. Standard CMR protocol included multislice, multidirectional survey images, steady-state free precession (SSFP) cine gradient-echo sequences at two-, three-, and four-chamber views, and short-axis slices covering the left ventricle from base to apex. For all sequences, coil-element combination was automatically determined for efficient signal-to-noise ratio (SNR) in the selected field of view (FOV), with measured coil sensitivity in the reference scan at the beginning of the examination for each patient [12]. All patients gave written informed consent before each magnetic resonance imaging (MRI) examination.

MOLLI MRI

All T1 acquisitions were based on the modified MOLLI pulse sequence with balanced steady-state free-precession (SSFP) readout [9]. The recently proposed 5s(3s)3s and 4s(1s)3s(1s)2s schemes were applied for pre- and 20-min post-contrast (Gadovist 0.1 mmol/kg) T1 measurements, respectively [13]. The native MOLLI protocol consisted of two IR-prepared ECG-gated acquisitions (typically 8–14 images in total) separated by an interval lasting a minimum of 3 s to ensure full recovery of longitudinal magnetization, all performed within one breath-hold. Similarly, the post-contrast MOLLI protocol consisted of three IR-prepared acquisitions with two intervals of at least one second interspersed in between. Images were acquired at the basal and mid-cavity short-axis levels of the left ventricle, and all (both pre- and post-contrast) were timed to the mid-diastolic phase of the cardiac cycle and performed at end expiration. Imaging parameters were: (FOV 340 × 340 mm^2, matrix size 188 × 168, acquired pixel size 1.8 × 2.0 mm^2, interpolated pixel size 1.3 × 1.3 mm^2, slice thickness 8 mm, repetition time (TR) 2.3 ms, echo time (TE) 1.15 ms, flip angle (FA) 30°, minimal interval time TI delay 87.7 ms, bandwidth 1136.5 Hz/pixel, partial Fourier factor 0.8, sensitivity encoding (SENSE) factor 2.2, scan time ~11- to 13 s [14]. Simplified pulse sequence diagrams are shown in Supplementary Fig. 1.

Motion correction and co-registration

A modified nonrigid, nonparametric image registration method was applied to generate motion-corrected MOLLI image series and subsequently to co-register the native and post-contrast T1 maps [15]. In principle, motion estimation between two images is known as an image registration or co-registration task. Given two images, a registration algorithm aims to find a displacement vector field such that its application to the first image results in a new deformed image being most similar to the second image. While this procedure is directly applicable to the alignment of native and post-contrast T1 maps, it can also be used to generate the motion-corrected MOLLI image series such that one designated image out of the series is defined as a reference frame, to which all remaining images are aligned subsequently. For motion correction of a MOLLI CMR image series, the last time frame with the longest inversion time was used as the reference image. For co-registration of native and post-contrast T1 maps, the former was used as reference image. The mathematical framework is detailed as follows:

Given two images R, T defined on an image domain Ω (here a subset of $\mathbb{R}^2$), a registration algorithm aims to find a displacement field $u : \Omega \to \mathbb{R}^2$ such that $T(id + u)$ is most similar to R. In mathematical terms, the similarity is described by a function $\mathcal{D}[u, R, T]$, here chosen as the normalized gradient field (NGF),

$$\mathcal{D}[u, R, \mathrm{T}] = \frac{1}{2} \int_{\Omega} 1 - \langle n(R, x), n(T, x + u) \rangle^2 \mathrm{d}x, \tag{1}$$

where the term $n(I, x)$ describes the normalized image gradient of an image I at position x, and is given by $n(I, x) := \frac{\nabla I(x)}{\|\nabla I(x)\|_\varepsilon}$ with $\| x \|_\varepsilon := \left(x_1^2 + x_2^2 + \varepsilon^2\right)^{1/2}$. ε is introduced not only to avoid a division by zero but also to control what can be interpreted as a significant difference to separate image noise from valuable information. It is chosen in relation to the total mass of edges in the image by computing the spatial gradient of the input image, taking its modulus and integrating over the entire image domain.

A registration based only on a similarity measure may yield a deformed template image that perfectly matches the reference image as long as all intensity values are present in both images. However, the problem is ill-posed, and the underlying deformation in general may not be applicable in a physical context. Therefore, an additional smoothness constraint (or regularizer) is considered, which can be chosen to model application-specific physical properties. It should be noted that the regularization term also serves as a check for the resulting vector field against unwanted physiologically implausible behaviors (e.g., strong local expansion, compression, or even folding). In addition, with regularization, the registration algorithm is less affected by image noise, imaging artifacts or abrupt change of contrast (e.g., caused by IR). In our experiments, we employed a regularizer based on the popular linear elastic potential

$$\mathcal{S}[u] = \int_{\Omega} \left(\frac{\mu}{4} \sum_{k,l=1}^{2} \left(\partial_{x_k} u_l(x) + \partial_{x_l} u_k(x) \right)^2 + \frac{\lambda}{2} (\nabla \cdot u(x))^2 \right) \mathrm{d}x. \tag{2}$$

Its elastic properties are modeled by Lamé parameters λ, μ, which can be translated into Young's modulus (linked to tissue stiffness) and Poisson's ratio (contraction perpendicular to applied stretch). Specifically, μ is inversely proportional to the elastic modulus and λ/μ is proportional to the incompressibility of the material. To address respiratory and cardiac motions during the scan procedure, on the one hand, and the inflow of contrast agent on the other hand, a relatively large Young's modulus and small Poisson's ratio were chosen. As is common with registration algorithms, absolute values from the literature cannot be used, since their choice depends on the intensity scale of the acquired scans, the chosen similarity measure, and implementation issues.

By combining the similarity measure and the regularizing term, the problem can be formulated as finding a displacement field u, which minimizes the joint function

$$\mathcal{T}[u, R, T] = \mathcal{D}[u, R, T] + \mathcal{S}[u]. \tag{3}$$

The computation of the Gâteaux derivative of Eqs. (1) and (2) yields a necessary condition for u being a minimizer of Eq. (3). The outcome is a system of nonlinear partial differential equations equipped with associated boundary conditions. For its discretization, finite differences in conjunction with Neumann boundary conditions were chosen. The resulting system of linear equations consists of, on the one hand, a sparse, symmetric, and highly structured matrix arising from the regularizer and, on the other hand, a so-called force vector corresponding to the similarity measure. The system of equations is then linearized and iteratively solved by a conjugate gradient scheme. The iteration is stopped if the update in u is below some threshold for all positions indicating convergence. To ensure convergence and to increase robustness, the algorithm was embedded into a multiresolution scheme. This means that for each input frame, a pyramid of images is created consisting of the image at original resolution and its down-sampled copies at coarser resolutions. The registration starts at the coarsest resolution level. As soon as convergence is reached, the optimized displacement field is up-sampled to the next finer-resolution level and used as the starting point for registration on this level. This process is repeated until the finest resolution level is reached. Such a multiresolution scheme not only speeds up the entire registration process, since most computations are done on smaller images, it also increases robustness and convergence

speed, with the major structures aligned first, followed by the more granular structures.

Myocardial T1 and ECV mapping

By obtaining the motion-corrected MOLLI series, the T1 map was generated via the pixel-wise curve fitting using the three-parameter signal model [17] (Eq. 4).

$$S(t) = A - B \cdot e^{-\frac{t}{T1^*}}. \tag{4}$$

$S(t)$ described the measured T1 signal, while the unknown parameters (A, B, T1*) at each pixel was fitted using the Levenberg–Marquardt minimization [18] algorithm. The obtained apparent T1, denoted as T1*, was then corrected for signal saturation according to [17]

$$T1 = \left(\frac{B}{A} - 1\right) \cdot T1^*. \tag{5}$$

Contouring the epi- and endomyocardial borders was done manually. Further blood-pool segmentation was achieved based on native T1 map using a threshold of 1400 ms, as T1 of the pre-contrast blood ranges between 1600 and 2200 ms at 3T [3]. The ECV map was generated based on co-registered native and post-contrast T1 maps and individual hematocrit measured on the same day of the CMR examination [7, 19, 20]. For comparison, an additional ECV map was generated for each case based on motion-corrected T1 maps but without co-registration. Median native and post-contrast blood T1 values were used in the calculation of ECV according to:

$$ECV = \frac{\Delta R1_{\text{myocardium}}}{\Delta R1_{\text{blood pool}}} \cdot (1 - \text{hematocrit}). \tag{6}$$

where

$$\Delta R1 = \frac{1}{T1_{\text{post}}} - \frac{1}{T1_{\text{pre}}}. \tag{7}$$

The whole procedure followed the recently published consensus statement [5]. In addition, a T1-fitting error map with a unit of milliseconds was produced based on the estimated standard deviation (SD) of the corresponding T1-map value at each pixel, as proposed by [16]. Meanwhile, an overlay map was generated from a pair of native and post-contrast T1 maps for quality evaluation [14]. All calculation was done offline using a Matlab program developed in-house (The Mathworks, Natick, MA, USA). The entire process is shown in Fig. 1 as a straightforward approach.

Evaluation

Performance of motion correction and image co-registration was evaluated both qualitatively by visual inspection and quantitatively. First, two observers (1 cardiologist and 1 cardiac imaging scientist with 10 and 5 years of experience, respectively) assessed the quality of T1 (native and post-contrast) and ECV maps based on the generated error and overlay maps, respectively. A 3-point ordinal score (1 = good quality, 2 = fair quality and 3 = poor quality) was used for all cases, independent from motion compensation. Subsequently, by comparing scores, the performance of the motion correction and co-registration was categorized as either improved, maintained, or deteriorated.

In addition, to evaluate the co-registration performance of native and post-contrast T1 maps for ECV mapping, the local deformation vector field $\varphi(x) = x + u(x)$, $x \in \Omega$ was generated as an output from the registration algorithm. It established a pixel-wise correspondence between the two input images; i.e., it described for every pixel x in the one image a vector pointing to the corresponding anatomical position $x + u(x)$ in the other image. Based on that, a qualitative local deformation field (LDF) map and a quantitative local volume change (LVC) map were calculated. The LDF map was calculated as $\text{LDF}(x) := C(\varphi(x))$, $x \in \Omega$, with $C : \Omega \to \mathbb{R}^2$ being a checkerboard image, which was used to visualize local deformation. Meanwhile, as LVC was mathematically defined as the determinant of the Jacobian of the deformation vector field, for each pixel x of a 2D image, it was computed as $\text{LVC}(x) := \det(\nabla\varphi(x)) - 1$, with the spatial derivatives of φ evaluated in a small environment, consisting of 3×3 pixels in this work, to quantify the local volume change, including compression and expansion. A value of 0 indicated volume preservation, while a positive value was defined as expansion and a negative value as compression, not considering the through-plane motion. Both LDF and LVC maps were overlaid with the isocontour of the native T1 map as reference for visual guidance. An example underlining the principle was given in Supplementary Fig. 2 using numeric simulation.

Myocardial T1 and ECV values were measured by placing a region of interest (ROI) conservatively within the short-axis left-ventricular myocardium at the mid-myocardial region to avoid contamination by the blood pool. In addition, focal lesions with positive late gadolinium enhancement (LGE) were excluded from the ROI.

Statistics

Data were presented as percentages for categorical variables and mean ± SD for continuous variables. The distribution of all continuous variables was tested for normality using the Shapiro–Wilk test. Intra- and inter-observer reproducibility before and after motion correction and co-registration were assessed using Bland–Altman analysis and intraclass correlation coefficients (ICC). All statistical analyses were

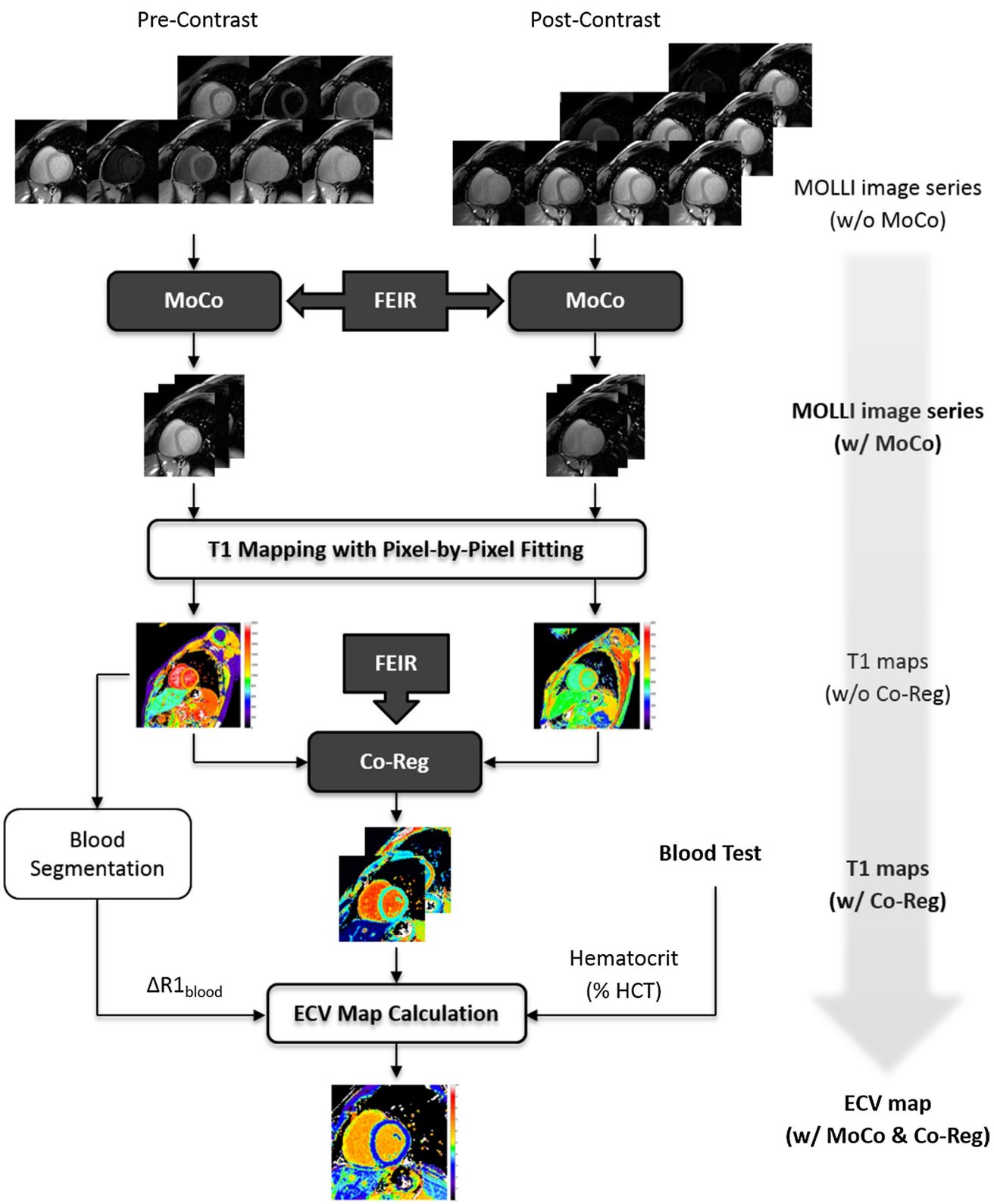

Fig. 1 Workflow of T1 and extracellular volume (ECV) mapping combined with motion correction and co-registration using the proposed approach. *MoCo* motion correction, *Co-Reg* co-registration. For details, see text

performed using IBM SPSS Statistics version 17. A $P < 0.05$ was considered statistically significant.

Results

We analyzed 82 myocardial T1 maps (pre- and post-contrast basal and mid-cavity slices) from 21 patients with diverse cardiac pathologies: cardiomyopathies [dilated cardiomyopathy (DCM), $n = 6$; hypertrophic cardiomyopathy (HCM), $n = 3$; restrictive cardiomyopathy, $n = 4$), ischemic heart disease (IHD) with infarct ($n = 6$), and hypertensive heart disease ($n = 2$)].

T1 mapping with motion correction

Table 1 summarizes the performance of motion correction on T1 mapping. Motion correction improved the quality in 59% of all maps, with a trend toward greater improvement in the post-contrast case compared with the native case ($P = 0.07$). Overall, there was an increase in good cases, from ~10% (8/82) to 48% (39/82), and a decrease of poor cases, from 23% (19/82) to 2% (2/82). Only two native cases exhibiting poor quality did not show improvement and were removed from further processing and quantitative analysis. No maps deteriorated in quality after motion correction. Selected clinical examples are presented in Figs. 2 and 3 of patients with DCM and IHD. In general, myocardial structure and shape were more aligned in the motion-corrected T1 maps with less signal variations across the myocardium. Meanwhile, there were less-visible fitting errors, as shown in error maps. A separate example with manual myocardium segmentation in video format can be found in the Supplementary Movie 1.

Myocardial T1 values of 1280 ± 51 ms native and 597 ± 73 ms post-contrast were obtained after motion correction. Reduced T1 fitting errors were found across all patients after motion correction (Supplementary Table 1).

ECV mapping with co-registration

Based on motion-corrected native and post-contrast cardiac T1 maps, co-registration further improved the quality of ECV maps in 67% of the 39 cases and 85% of poor cases (Table 2). Ten ECV maps improved from poor to good, whereas three remained poor after co-registration. Two corresponding examples are shown in Fig. 4. Similar to motion correction, myocardial structure and shape appeared more intact in the co-registered ECV map, with less intensity variations across the myocardium.

In regard to evaluation of the co-registration performance, generally only mild and smooth local deformation was observed, as indicated by the slightly deformed checkerboard grids in the LDF maps (Fig. 5). Meanwhile, only small local volume change (≤ 10% for myocardium) was found for most of cases, indicating good volume preservation.

In these patients with cardiac pathologies, global ECV with co-registration was 34.8 ± 7.0%, slightly higher than without co-registration (33.5 ± 7.6%). For details, see Supplementary Table 1.

Reproducibility

In general, the proposed motion correction and co-registration approach resulted in improved intra- and inter-observer agreement, as presented in Fig. 6. A detailed summary showing decreased differences and higher intraclass correlation coefficients (ICC) can be found in Supplementary Table 2.

Discussion

A method of motion correction and co-registration for myocardial T1 and ECV mapping was proposed and validated using patient data. The novel algorithm based on a fully automatic, nonrigid, nonparametric, image registration approach provides a robust solution, with improved precision and reproducibility and simplified workflow despite the widely varying contrast across the multiple inversion-recovery source images.

We show that this approach leads to improved image quality in 67% of all cases and 85% of poor cases and reduces errors without image quality deterioration. The average values of T1 and ECV before and after motion correction and co-registration differed only by a few milliseconds or percent points that, although statistically significant, may be deemed clinically insignificant (Supplementary Table 1). Of note, we demonstrate improved intra-observer reproducibility and

Table 1 Evaluation of motion correction (MoCo) performance for T1 mapping

	Native ($n = 41$)			Post-contrast ($n = 41$)			Total ($n = 82$)		
	Poor	Fair	Good	Poor	Fair	Good	Poor	Fair	Good
w/o MoCo	9	27	5	10	28	3	19	55	8
w/ MoCo	2	21	18	0	20	21	2	41	39
Improvement	78%	–		100%	–		89%	–	
	49% (20/41)			68% (28/41)			59% (48/82)		

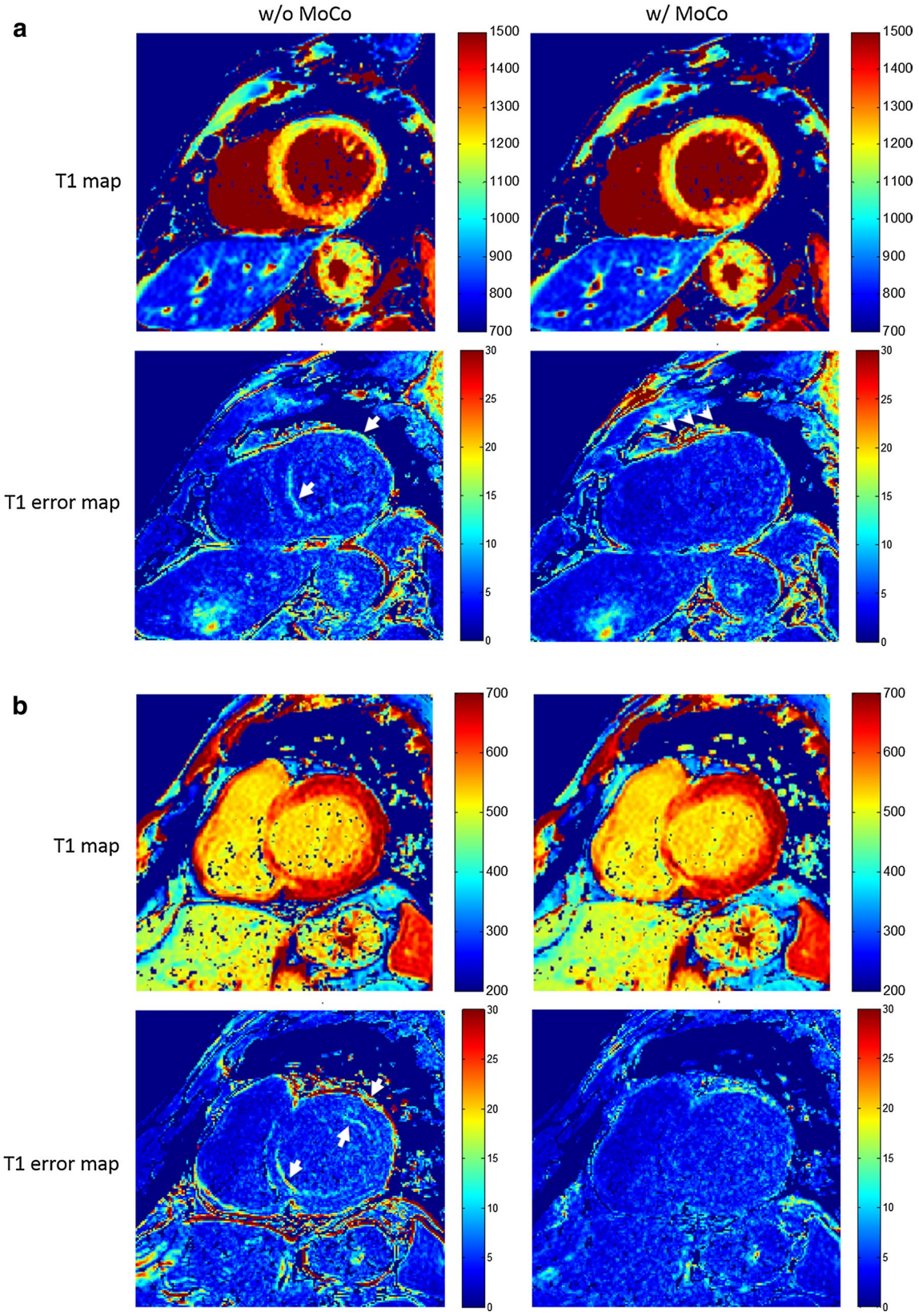

Fig. 2 Motion correction for T1 mapping with quality improvement. Short-axis mid native (**a**) and basal post-contrast (**b**) ventricular T1 (top row) and fitting error (bottom row) maps of one patient with dilated cardiomyopathy (DCM) before (left column) and after (right column) motion correction. Myocardial structure showed better alignment compared with obvious fitting error at the septal (**a**) and septal-to-anterior (**b**) subendocardial segments without motion correction (white arrow)

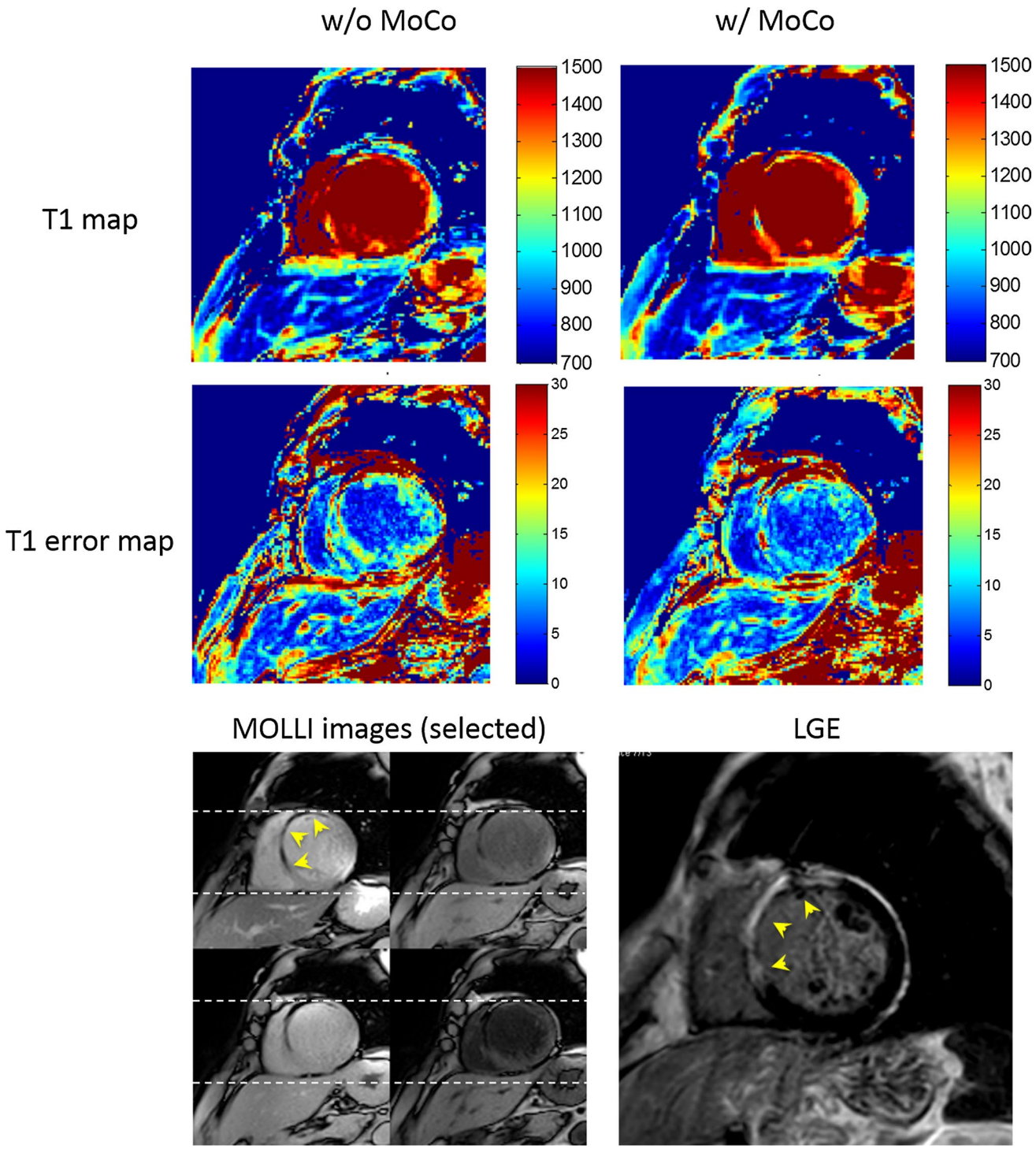

Fig. 3 Motion correction for T1 mapping without quality improvement (from poor to poor). Short-axis mid ventricular native T1 (top row) and fitting-error (middle row) maps of one patient with ischemic heart disease (IHD) before (left column) and after (right column) motion correction. Selected modified look-locker inversion recovery (MOLLI) images (4 out of 8) showed both great motion (dotted lines) and extensive infarct, which was consistent with the late gadolinium enhancement (LGE) image (arrowheads). Two out of 82 cases remained of poor quality with motion correction and were inadequate for contouring and were thus excluded for quantitative analysis. See text for details

Table 2 Evaluation of co-registration (Co-Reg) performance for ECV mapping

	Poor	Fair	Good
w/o Co-Reg ($n = 39$)	20	15	4
w/ Co-Reg ($n = 39$)	3	13	23
Improvement	85%	–	
	67% (26/39)		

inter-observer agreement by using the proposed method. This has important implications for reliable measurement for delineating the ranges in health and disease, as well as longitudinal surveillance of disease progression or treatment response. Additionally, increased precision translates into the need for fewer sample numbers to demonstrate statistical differences in research studies [24].

A different approach reported previously computes a synthetic MOLLI series based on estimated T1 IR signal for intra-series motion correction and further generates individually corrected post-contrast images based on a composite motion deformation field for inter-series co-registration in an iterative manner [10, 11]. Its advantage was demonstrated by comparison with a direct, nonrigid co-registration method using local cross correlation for image-similarity measure and regularization of the velocity of the displacement, which—while offering more flexibility in terms of deformation—may lead to undesired distortion. In contrast, the proposed method here applies normalized gradient field (NGF) for similarity measure and the Navier-Lamé operator as a regularizer. While the former tries to align edge orientation regardless of the direction and extent of intensity changes (described below), the latter was strongly weighted to restrict elasticity and avoid large local deformation. In addition, the proposed method applies a straightforward and stepwise process to produce motion-corrected T1 and ECV maps without iterative computation or synthetic image estimation (Fig. 1). This greatly simplifies workflow and computational demands and avoids error propagation that may occur at any (pre-) processing step. Because the correction method is independent of the outcome measure (in this case, T1 estimation), the technique can be easily extended to other MOLLI schemes, signal readouts, and even free-breathing applications [22]. In terms of computational demand, for co-registration of two 2D images (e.g., with a matrix size of 352 × 352 pixels), this method requires 0.13 s, while for alignment of 8–14 images, it typically requires 0.9–1.7 s.

The optimized MOLLI sequences with the recently proposed second-based schemes were used in this work to measure pre- and post-contrast myocardial T1 relaxation times. In comparison with the original schemes defined in beats, scan time depends less on heart rate and allows better sampling of the relaxation curve at high heart rate [13, 16]. While a thorough investigation of this scheme is beyond the scope of this study, which focused on motion correction and co-registration, two examples of pulse sequence diagrams with different heart rates are shown in Supplementary Fig. 1 for native and post-contrast T1 mapping, respectively. In addition, a moderate FA of 30° was used for reduced off-resonance sensitivity with sufficient SNR on 3T [13, 21].

The task of aligning two images during motion correction or co-registration processes requires a definition of similarity in mathematical terms. For images in which the intensity describes a quantity, such as absorption in computed tomography (CT) data, this approach is valid. For other imaging modalities, such as MRI, positron emission tomography/single-photon emission tomography (PET/SPECT), or ultrasound (US) imaging, intensities will vary. Mutual information is often described as a similarity measure suited for multimodal registration applications. When studying the way a human observer inspects and compares images, attention focuses on image structures rather than intensities. Such structures are described by image edges. Two images appear similar to each other if edges occur at the same spatial positions, and edges are similar to each other if their spatial image gradients are similar. In this work, the similarity measure was done by using NGF [23]. Although NGF relies on edge structures, its advantage here is that the orientations of the gradient vectors do not have to be the same in order to allow intensity gradients from bright to dark to match with those from dark to bright. In addition, the amplitudes of the gradient vectors do not need to be similar, so that less-contrasted edges can match with more distinctive edges. This is a necessity of the MOLLI image series, where image intensities and contrasts can change drastically during IR. Therefore, unlike previous work in motion compensation for myocardial perfusion, where multiple computed images were used as templates or reference frames due to their gradual contrast uptake in different tissue compartments [25, 26], only one image—typically the last time frame—from the MOLLI series was used as the reference in this work.

A similar image registration approach was previously applied in CT and PET imaging for 3D data, where the sum of squared differences (SSD) were used as similarity measure [15]. In our work, this was replaced by NGF, and the framework was modified and extended for co-registration of multiple 2D images, and is applied in quantitative cardiac MR parametric mapping. While there was a nearly five-fold increase in good cases and 12-fold decrease in poor cases for motion correction of the MOLLI series (Table 1), 67% of cases demonstrated further qualitative improvement for ECV mapping with co-registration of native and post-contrast T1 maps. In both scenarios, no quality deterioration was observed. Qualitative image assessment suggests better myocardial alignment with fewer errors at the endocardial and epicardial borders with motion correction compared

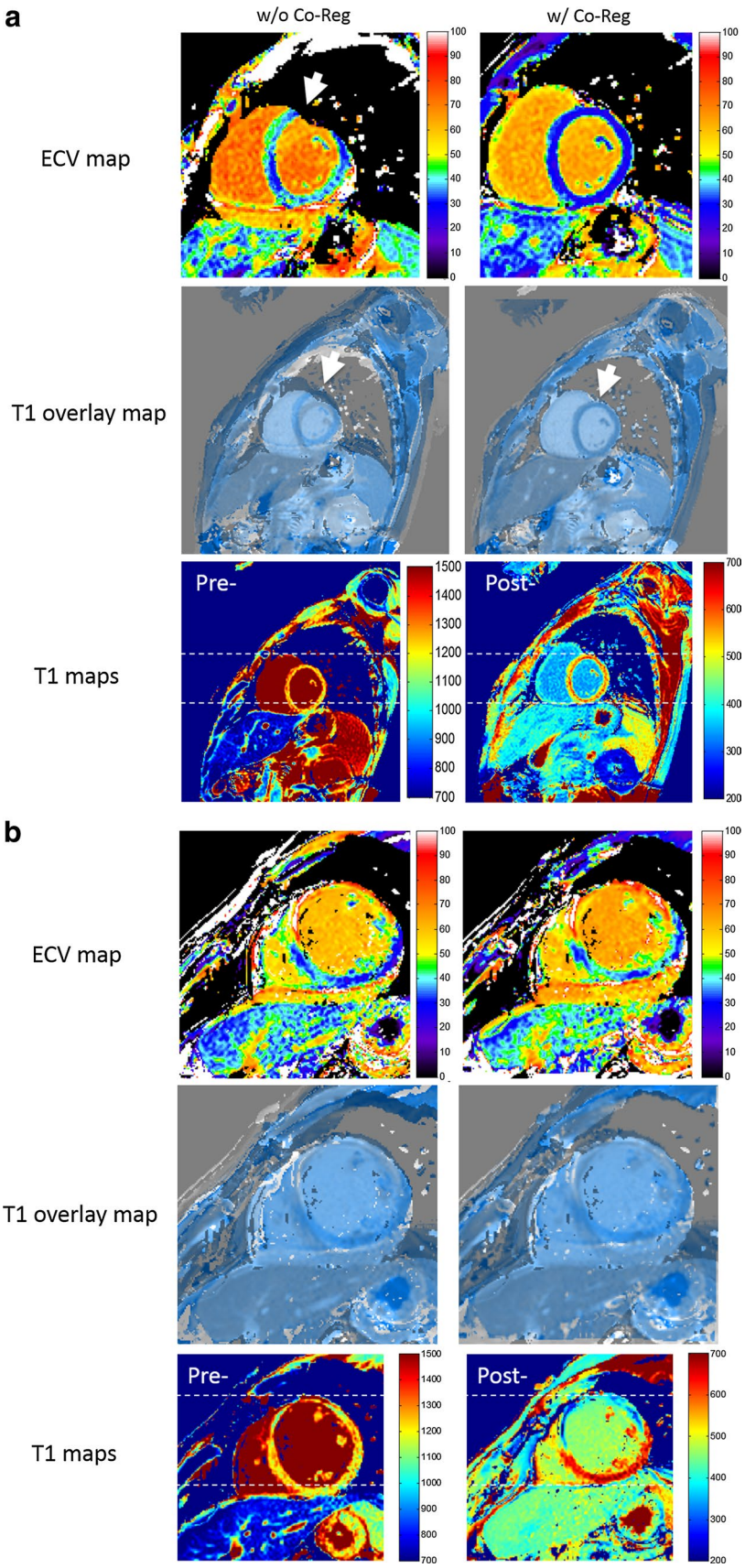

Fig. 4 Image co-registration for extracellular volume (ECV) mapping with (**a**) and without (**b**) quality improvement. Short-axis basal ventricular ECV (top row) and native and post-contrast T1 overlay (second row) maps before (left column) and after (right column) image co-registration (Co-Reg) in two patients (**a**, **b**) with ischemic heart disease. The individual native and post-contrast T1 maps are shown side-by-side (last row), respectively. In (a), obvious misalignment seen in the T1 overlap map (white arrows) and individual native and post-contrast maps (dotted lines) was corrected with co-registration that yielded a more homogenous ECV map. In (**b**), image co-registration did not improve interpreter-assessed quality of the ECV map. Distinct motion status (dotted lines) with myocardial infarct involving the anterior and anteroseptal walls was appreciated in greater relief in the post-contrast compared with native T1 map (last row)

to without (arrows in Fig. 2). More fitting errors were visible outside the heart after motion correction in this example (arrowheads in Fig. 2) but were not seen in other cases. These observations may need to be investigated in a larger cohort. Robustness and accuracy can be further demonstrated in LDF and LVC maps. In nonrigid registration, a small and smooth local deformation is often desired to avoid unwanted distortions and possible image deterioration. The computed local deformation field was used in this work to generate two independent maps for assessing the co-registration performance both qualitatively and quantitatively. In general, only mild and smooth local deformations were found in all cases (as shown by the LDF maps in Fig. 5). In particular, we did not observe a local mixed pattern of compression and expansion. A global translation neither deforms vertical or horizontal lines nor changes the size or shape of any checkerboard grids. In contrast, a local deformation may result in deformed lines and even, in case of volume change, expanded or compressed checkerboard grids. In addition, LVC was close to 0 ($\leq 10\%$) in the myocardium, which indicated good volume preservation. Relatively larger changes ($\geq 10\%$ but $\leq 50\%$) were sometimes observed in either the blood pool or the lung, which might indicate different respiratory statuses and/or cardiac phases between two T1 maps (LVC maps in Fig. 5).

Two cases of motion correction of MOLLI series and three of co-registration for ECV mapping showed no improvement and remained of poor quality (Figs. 3 and 4). In these cases, both greater in- and through-plane motions and focal infarcts were observed. While such focal pathologies limited in spatial extent may not be captured in the 2D frame due to through-plane motion [27], they may lead to substantially differently recognized structural shapes that violate the physiologically plausible behavior the regularizing term is based on in the elastic modeling, thus constituting the main cause of a failed measure for similarity. It is worth mentioning that in this case, local deformation maps may not fully address the challenge, as other than misalignment of focal lesions, both in- and through-plane motions, will appear as overall mild volume changes. However, co-registration is, by design, mainly capable of correcting for in-plane motion and does not address new features or tissue structures introduced by through-plane motion.

The combination of motion correction and co-registration not only allows for more robust alignment of the myocardial structures but also improves precision for T1 calculation, as shown by the reduced T1 fitting errors (Supplementary Table 1) and better intra- and inter-observer reproducibility (Fig. 6 and Supplementary Table 2). In addition, it helps improve the workflow for ECV mapping. A pixel-by-pixel calculation of the ECV map provides direct visualization and may facilitate easy interpretation for clinical studies. Further technical improvement will focus on parameter optimization, computational power, synthetic ECV mapping without hematocrit [28, 29], and, in particular, an integrated process. A straightforward and stepwise procedure of the proposed method also facilitates easy integration of the algorithm on the MR scanner, in addition to its robustness against large variations of image contrast throughout IR.

This initial report may pave the way for a more comprehensive evaluation of the proposed method on a larger clinical cohort. Moreover, the proposed method may be extended to other parametric mapping and to free-breathing image series, such as perfusion or cine data, which need to be investigated in future studies.

This work has several limitations. First, this was an exploratory study on the technical feasibility of the proposed method, and only a small number of patients was included. Nevertheless, we demonstrate enhanced reproducibility of T1 and ECV measurements by motion correction and co-registration, respectively. Second, diverse cardiac pathologies were studied. Relatively higher T1 and ECV values were found in the cohort in comparison with those previously reported [30, 31] but cannot be taken to be representative of individual pathologies or considered as normal ranges, as values are predictably affected by different flip angles and other variations in vender-specific implementation. Due to scan-time restriction, only the aforementioned second-based MOLLI scheme was used in this study. A thorough investigation of it in comparison with other existing methods may be warranted in a larger clinical cohort. Moreover, in common with all motion correction and co-registration techniques, blood signal contamination in the myocardium is a source of potential error. In the current work, this error was minimized by manual ROI definition, including only the mid-myocardial region for analysis, leaving a wide margin at the epicardial and endocardial borders. In addition, image smoothing and through-plane motion remain challenging problems for all image registration methods, and further studies are needed. Focal macrofibrosis evident on LGE images that are likely to be present in some patients may result in heterogeneous regional T1 measurements within the slice, which was not specifically addressed in this study. A local reference based on the same sequence settings needs to be established to further investigate its clinical significance; however, it was not the focus of this study. Finally, the presence of irregular heartbeats may degrade image quality, which has neither

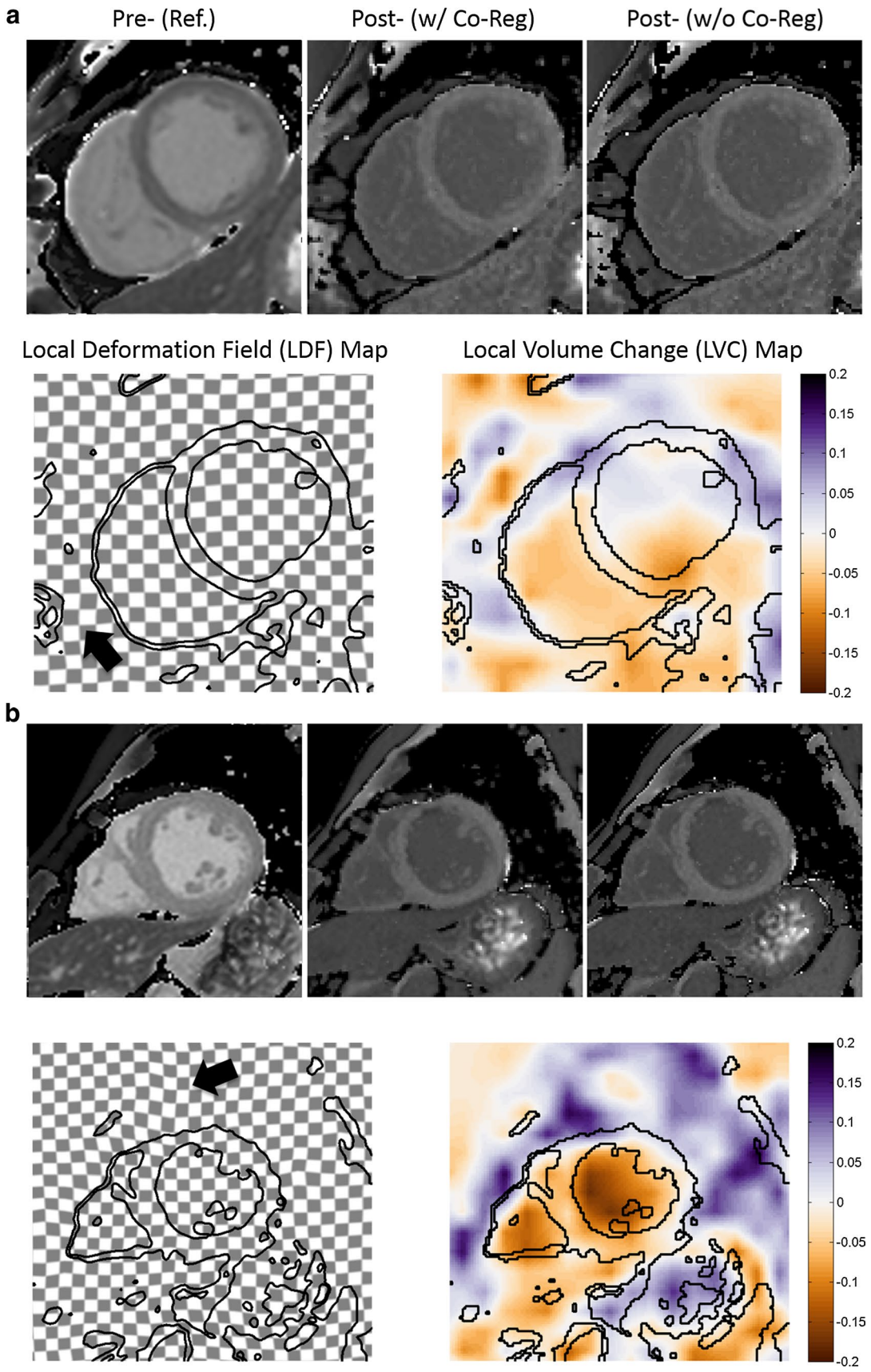
a
Pre- (Ref.)
Post- (w/ Co-Reg)
Post- (w/o Co-Reg)
Local Deformation Field (LDF) Map
Local Volume Change (LVC) Map
0.2
0.15
0.1
0.05
0
-0.05
-0.1
-0.15
-0.2
b
0.2
0.15
0.1
0.05
0
-0.05
-0.1
-0.15
-0.2

◂**Fig. 5** Image co-registration for extracellular volume (ECV) mapping with quality maintained. Short-axis mid ventricular T1 maps (top row), local deformation field (LDF) map (bottom left), and volume change map (bottom right) in two patients (**a**, **b**) with ischemic heart disease. For co-registration, the native T1 map (top left) served as reference and the post-contrast T1 map (top right) as target; the final map is displayed (top middle). In both cases, only small and smooth deformation were found in both the LDF checkerboard by slightly deviated vertical or horizontal lines (arrows) and local volume change (LVC) map (≤ 20%). See text for details

been investigated in this study nor in works by others on MOLLI-based sequences.

Conclusion

This work describes a robust motion correction and co-registration method for both myocardial T1 and ECV mapping based on a fully automatic, nonrigid,

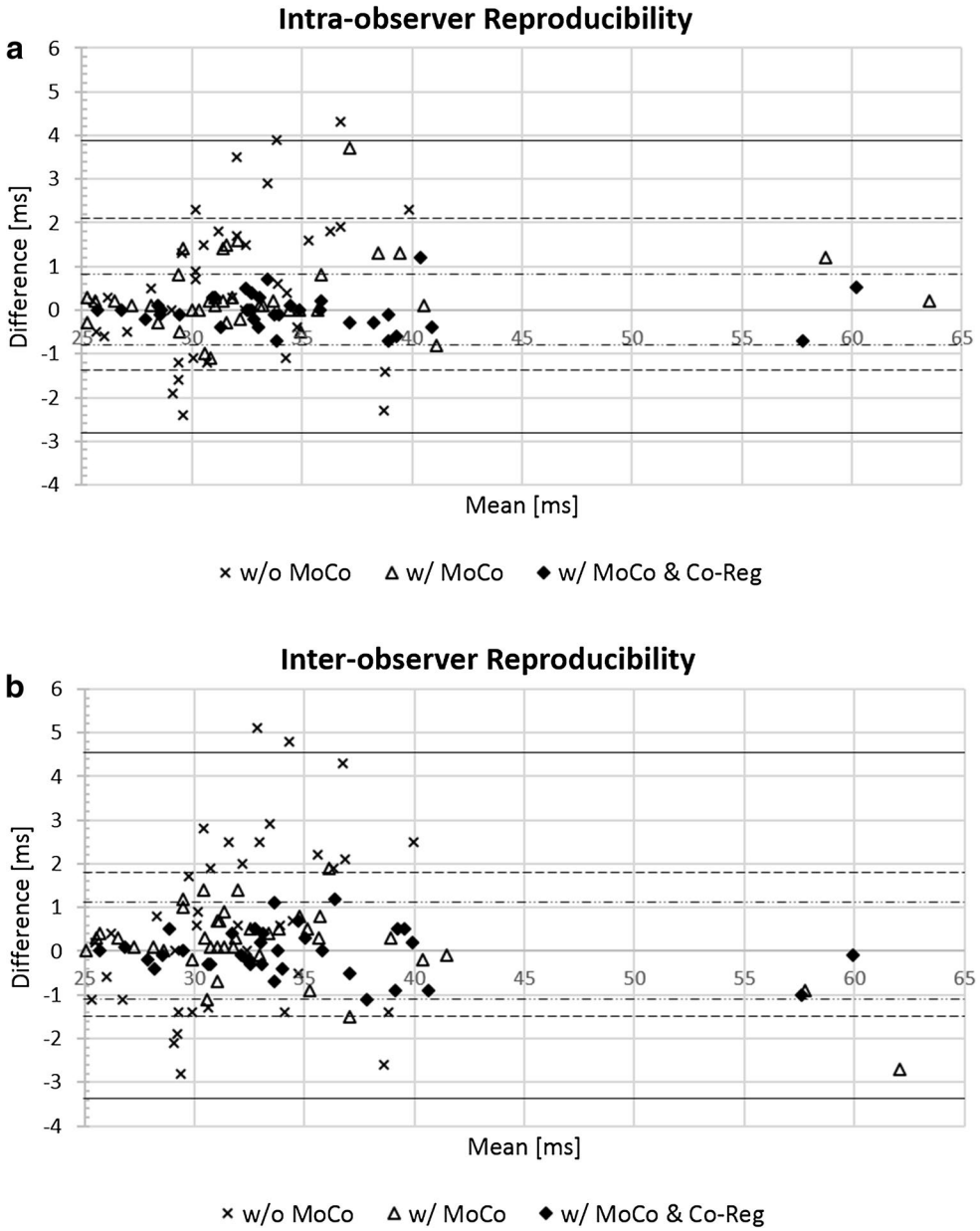

Fig. 6 Intra- (**a**) and inter-observer (**b**) reproducibility of extracellular volume fraction (ECV) measurements without and with motion correction and co-registration. Bland–Altman plots of measured ECV values at the mid- and basal levels (n = 82 cases), with 95% limits of agreement (LOA) superimposed on the chart for without motion correction or co-registration (w/o MoCo, solid lines), with motion correction only (w/MoCo, dashed line), and with both motion correction and co-registration (w/MoCo and CoReg, dash–dotted line). Improved agreement was found using the proposed method, as shown by the decreased differences and tighter 95% LOA

nonparametric, image registration approach. Improved image quality, precision, and reproducibility have been demonstrated. The simple workflow allows for seamless integration into the image acquisition and reconstruction pipeline for future clinical practice. Further research is needed to validate aspects of both novel MOLLI variants and the proposed motion compensation approach in a larger cohort.

Acknowledgements The authors would like to acknowledge Bao Ru Leong, Yiying Han, Yi Hui Hung, and Elizabeth Goh Pee Chong for their support in acquiring CMR data, and Xiaodan Zhao for her help in statistical analysis.

Author contribution SZ helped to conceive the study, developed the nonproprietary program in Matlab for T1 and ECV mapping, performed processing, and drafted the manuscript. TTL helped to conceive the study, helped to develop the program for T1 and ECV mapping, and performed processing and analysis. SK developed motion correction and co-registration algorithm and program, and drafted the manuscript. BS helped to develop the program for T1 and ECV mapping. DJH and SAC participated in design of the study. RST and CWLC conceived of the study, performed processing and analysis, and drafted the manuscript. All authors read and approved the final manuscript.

Compliance with ethical standards

Conflict of interest SZ and SK are Philips employees.

Ethical standards All procedures performed in studies involving human participants were in accordance with the ethical standards of the institutional and/or national research committee and with the 1964 Helsinki Declaration and its later amendments or comparable ethical standards. Informed consent was obtained from all individual participants included in the study.

Funding DJH was supported by the British Heart Foundation (FS/10/039/28270), the Rosetrees Trust, and the National Institute for Health Research University College London Hospitals Biomedical Research Centre.

References

1. Schaper J, Speiser B (1992) The extracellular matrix in the failing human heart. Basic Res Cardiol 87(Suppl 1):303–309
2. Mewton N, Liu CY, Croisille P, Bluemke D, Lima JA (2011) Assessment of myocardial fibrosis with cardiovascular magnetic resonance. J Am Coll Cardiol 57:891–903
3. Chin CWL, Semple S, Malley T et al (2014) Optimization and comparison of myocardial T1 techniques at 3T in patients with aortic stenosis. Eur Heart J Cardiovasc Imaging 15:556–565
4. Wong TC (2014) Cardiovascular magnetic resonance imaging of myocardial interstitial expansion in hypertrophic cardiomyopathy. Curr Cardiovasc Imaging Rep 7:9267–9273
5. Moon JC, Messroghli DR, Kellman P et al (2013) Myocardial T1 mapping and extracellular volume quantification: A Society for Cardiovascular Magnetic Resonance (SCMR) and CMR Working Group of the European Society of Cardiology consensus statement. J Cardiovasc Magn Reson 15:92
6. Vesey A, Esson G, Chin C, Dweck M, Newby D (2015) Detection of cardiac fibrosis and cell death in patients with aortic stenosis. J Am Coll Cardiol. https://doi.org/10.1016/S0735-1097(15)61190-1
7. Flett AS, Hayward MP, Ashworth MT et al (2010) Equilibrium contrast cardiovascular magnetic resonance for the measurement of diffuse myocardial fibrosis: preliminary validation in humans. Circulation 122:138–144
8. Wong TC, Piehler K, Meier CG et al (2012) Association between extracellular matrix expansion quantified by cardiovascular magnetic resonance and short-term mortality. Circulation 126:1206–1216
9. Messroghli DR, Radjenovic A, Kozerke S, Higgins DM, Sivananthan MU, Ridgway JP (2004) Modified look-locker inversion recovery (MOLLI) for high-resolution T1 mapping of the heart. Magn Reson Med 52:141–146
10. Xue H, Shah S, Greiser A et al (2012) Motion correction for myocardial T1 mapping using image registration with synthetic image estimation. Magn Reson Med 67:1644
11. Kellman P, Wilson JR, Xue H, Ugander M, Arai AE (2012) Extracellular volume fraction mapping in the myocardium, part 1: evaluation of an automated method. J Cardiovasc Magn Reson 14:63
12. Buehrer M, Pruessmann KP, Boesiger P, Kozerke S (2007) Array compression for MRI with large coil arrays. Magn Reson Med 57:1131–1139
13. Kellman P, Hansen M (2014) T1-mapping in the heart: accuracy and precision. J Cardiovasc Magn Reson 16:2. https://doi.org/10.1186/1532-429X-16-2
14. Le TT, Zhang S, Kabus S, Leong BR, Han Y, Hausenloy DJ, Cook S, Tan RS, Chin CWL (2016) Extracellular volume fraction mapping at 3T with nonrigid image coregistration. J Cardiovasc Magn Reson 18(Suppl 1):P32
15. Kabus S, Lorenz C (2010) Fast elastic image registration. Proceeding of 13th meeting of medical image computing and computer-assisted intervention (MICCAI). Beijing, China, pp 81–89
16. Kellman P, Arai AE, Xue H (2013) T1 and extracellular volume mapping in the heart: estimation of error maps and the influence of noise on precision. J Cardiovasc Magn Reson 15:56
17. Deichmann R, Haase A (1992) Quantification of T1 values by SNAPSHOT FLASH NMR imaging. J Magn Reson 96:608–612
18. Marquardt DW (1963) An algorithm for least-squares estimation of nonlinear parameters. J Soc Ind Appl Math 11:431–441
19. Arheden H, Saeed M, Higgins CB et al (1999) Measurement of the distribution volume of gadopentetate dimeglumine at echo-planar MR imaging to quantify myocardial infarction: comparison with 99mtc-dtpa autoradiography in rats. Radiology 211:698–708
20. Ugander M, Oki AJ, Hsu L-Y et al (2012) Extracellular volume imaging by MRI provides insight into overt and subclinical myocardial pathology. Eur Heart J 33:1268–1278
21. Gai ND, Stehning C, Nacif M, Bluemke DA (2013) Modified look-locker T1 evaluation using Bloch simulations: human and phantom validation. Magn Reson Med 69:329–336
22. Zhang S, Okuaki T, Kabus S et al (2017) Free-breathing native cardiac T1 and T2 mapping with flexible elastic image registration: preliminary clinical result. In: Proceedings of the 25th scientific meeting of the International Society for Magnetic Resonance in Medicine, Honolulu p 2754

23. Haber E, Modersitzki J (2005) Beyond mutual information: a simple and robust alternative. In: Meinzer HP, Handels H, Horsch A, Tolxdorff T (eds) Bildverarbeitung fuer die Medizin 2005. Springer, Berlin, pp 350–354 **(ISBN 978-3-540-25052-4 (print)/978-3-540-26431-6 [online])**
24. Bellenger NG, Davies LC, Francis JM, Coats AJ, Pennell DJ (2000) Reduction in sample size for studies of remodeling in heart failure by the use of cardiovascular magnetic resonance. J Cardiovasc Magn Reson 2:271
25. Xue H, Zuehlsdorff S, Kellman P, Arai A, Nielles-Vallespin S, Chefdhotel C, Lorenz CH, Guehring J (2009) Unsupervised inline analysis of cardiac perfusion MRI. Med Image Comput Assist Interv 12(Pt 2):741
26. Milles J, van der Geest RJ, Jerosch-Herold M, Reiber JH, Lelieveldt BP (2008) Fully automatic registration and segmentation of first-pass myocardial perfusion MR image sequences. IEEE Trans Med Imaging 27:1611
27. Giri S, Shah S, Xue H et al (2012) Myocardial T2 mapping with respiratory navigator and automatic nonrigid motion correction. Magn Reson Med 68:1570
28. Treibel TA, Fontana M, Maestrini V et al (2016) Automatic measurement of the myocardial interstitium: synthetic extracellular volume quantification without hematocrit sampling. J Am Coll Cardiol: Cardiovasc Imaging 9:54
29. Fent GJ, Garg P, Foley JRJ, et al. Synthetic myocardial extracellular volume fraction (2017) J Am Coll Cardiol: Cadiovasc Imaging. (**ISSN 1936-878X**)
30. Rogers T, Dabir D, Mahmoud I et al (2013) Standardization of T1 measurements with MOLLI in differentiation between health and disease—the ConSept study. J Cardiovasc Magn Reson 15:78
31. Dabir D, Child N, Kalra A et al (2014) Reference values for healthy human myocardium using a T1 mapping methodology: results from the International T1 Multicenter cardiovascular magnetic resonance study. J Cardiovasc Magn Reson 16:69